AAS 14-453

ANALYTICAL SOLUTION FOR FLAT-SPIN RECOVERY OF SPINNING SATELLITES

Frank L. Janssens* and Jozef C. van der Ha†

The paper presents new analytical and numerical results in the field of self-excited rigid-body dynamics of spinning satellites. A practical solution for a flat-spin recovery maneuver is designed and evaluated. The proposed strategy uses a continuous body-fixed torque along the minor principal axis of inertia. The motion about the torque axis is similar to a pendulum which is either oscillating (i.e., no flat-spin recovery) or revolving (i.e., successful flat-spin recovery). The transition between these two cases defines the minimum required torque level. In the case when the recovery is successful the motion within the plane normal to the torque axis describes an ellipse with continuously growing angular velocity. The results established here are of considerable practical interest for the design of spacecraft that are required to spin about their minor axes of inertia due to launcher constraints or because of specific mission requirements.

INTRODUCTION

This paper presents new practical results in the field of self-excited spinning rigid-body dynamics[1-4] applied to satellite attitude motion[5-9]. A flat-spin recovery maneuver may well be the most striking practical example in this field. In the presence of energy dissipation, a satellite that is freely spinning about its minor principal axis of inertia is known to eventually end up spinning about its major axis of inertia[10-11]. For a satellite in a transfer orbit, it is of critical importance that the spin about the minor inertia axis is re-established before initiating the firing of the upper stage or apogee / perigee kick motor.

For the case when the applied constant body-fixed torque points along a principal axis of inertia it is known that this problem has a first integral[12] for the motion in the plane formed by the other two principal axes. This integral is a linear combination of the modulus of the instantaneous angular momentum and the rotational energy and is independent of the torque's magnitude. It leads to a straightforward solution in terms of the turning angle about the applied torque's axis.

This paper presents the detailed analysis for a torque about the minor principal axis of inertia and examines the effectiveness of this strategy in terms of the desired flat-spin recovery. Initially, the satellite is freely rotating about its maximum axis of inertia, either in a pure spin or with a specified level of nutation. The torque needs to increase the rotational energy relative to the instantaneous angular momentum in order that a rotation about the minor axis of inertia becomes feasible. Conversely, these results may also be formulated in terms of the maximum value of the angular velocity in flat-spin motion for a given torque level.

* Consultant, Wilhelminastraat 29, 2201 KA Noordwijk, the Netherlands; f.janssens@ziggo.nl.
† Consultant, 5808 Bell Creek Rd, Deming, WA 98244, USA; jvdha@aol.com.

On the basis of the first integral, we find another first integral that depends on the initial rotation rate about the minor inertia axis and the torque's magnitude. Next, the exact solution for the motion of the angular velocity in the principal body reference frame is established as function of the total turning angle about the minor inertia axis. The solution in terms of time reduces to a quadrature described by a generalized pendulum equation. The motion is similar to a pendulum which is either oscillating (no recovery) or revolving (recovery) with increasing angular velocity.

The minimum torque level that guarantees a flat-spin recovery occurs precisely at the transition between these two cases. The critical value of this torque level is derived from the solution for the angular velocity about the minor principal axis of inertia. If the transition from spinning about the z axis to spinning about the x axis occurs at all, it must take place during the first complete revolution of the angular velocity vector. A partial flat spin with a residual nutation has a higher rotational energy than a perfect flat spin so we would expect that a recovery can be performed with a smaller torque level. However, we find that the required torque depends on the nutation phase angle and may actually be higher or lower.

The analysis confirms that, in the case when the transition does take place, the nutation about the minor principal axis of inertia decreases from 90° to 0 as a consequence of the first integration constant. In fact, the amplitude of the rotational motion in the plane perpendicular to the torque remains constant whereas the angular velocity about the torque axis keeps growing as long as the torque acts. An averaging technique is used for determining the rate of decrease of the nutation.

The results presented here are of practical interest for the design of satellites that must spin about their minor axis of inertia because of launcher constraints or mission requirements.

DYNAMICAL MODEL

Equations of Motion

The motion of an asymmetric rigid body under a constant body-fixed torque is described by the Euler equations[11]:

$$\begin{aligned} A\dot{\omega}_1 + (C-B)\,\omega_2\omega_3 &= T_1 \\ B\dot{\omega}_2 - (C-A)\,\omega_1\omega_3 &= T_2 \\ C\dot{\omega}_3 + (B-A)\,\omega_1\omega_2 &= T_3 \end{aligned} \qquad \text{(1a-c)}$$

The dot denotes the time-derivative, ω_j are the components of the rotation vector $\boldsymbol{\omega}$ [rad/s] and the subscripts j = 1, 2, 3 refer to the x, y, z axes of the principal body frame. The torque vector **T** [Nm] acting on the body is expanded in its components T_j along the three principal body axes. Finally, A, B, C [kg m^2] stand for the principal moments of inertia in the following sequence:

$$A < B < C \qquad (2)$$

The structure of Eqs. (1) may be simplified by introducing the inertia coefficients:

$$k_1 = (C-B)/A; \quad k_2 = (C-A)/B; \quad k_3 = (B-A)/C \qquad \text{(3a-c)}$$

which satisfy $0 < k_j < 1$ (j = 1, 2, 3).

We introduce $t_j = T_j/I_j$ [rad/s^2] and I_j the moment of inertia about the corresponding axis we can write Eqs. (1) as:

$$\dot{\omega}_1 + k_1 \omega_3 \omega_2 = t_1$$
$$\dot{\omega}_2 - k_2 \omega_3 \omega_1 = t_2 \qquad (4a\text{-}c)$$
$$\dot{\omega}_3 + k_3 \omega_1 \omega_2 = t_3$$

We introduce the *instantaneous* (i.e., at an arbitrary time t) modulus $H(t)$ of the angular momentum vector $\mathbf{H}(t)$ and the rotational energy $E(t)$ of the system in Eqs. (1,4):

$$E(t) = \frac{1}{2}\left\{A\,\omega_1^2 + B\,\omega_2^2 + C\omega_3^2\right\}; \quad H^2(t) = \left\{A^2\omega_1^2 + B^2\omega_2^2 + C^2\omega_3^2\right\} \qquad (5a,b)$$

In the absence of external torques, both the energy and angular momentum are constants of the motion[11]. Figure 1 shows constant energy levels on the angular momentum sphere. In the presence of torques, the energy and angular momentum are *instantaneously* the same physical quantities as in the torque-free case but they become functions of time.

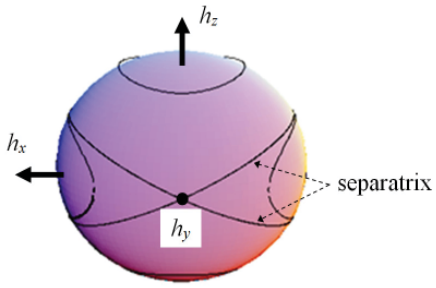

Figure 1. Constant Energy Levels on Angular Momentum Sphere.

Therefore, it follows from Eq. (2) that, for a given value $H(t)$, the corresponding energy $E(t)$ lies in the range:

$$E_{min}(t) = \frac{H^2(t)}{2C} < E(t) < \frac{H^2(t)}{2A} = E_{max}(t) \qquad (6)$$

The range of energy values in Eq. (6) can be separated in two intervals as shown in Figure 1:

$$a)\,motion\,about\,z: \quad E_{min}(t) < E(t) < \frac{H^2(t)}{2B} = E_{sep}(t) \qquad (7a)$$

$$b)\,motion\,about\,x: \quad E_{sep}(t) < E(t) < E_{max}(t) \qquad (7b)$$

where 'sep' denotes the separatrix, see Figure 1.

For illustration, we consider an arbitrary torque that has been acting during the interval $0 \le t \le t^*$ and terminates at time t^*. When the instantaneous values $E^* = E(t^*)$ and $H^* = H(t^*)$ satisfy Eq. (7a) the body continues to spin about its major inertia axis z. Alternatively, if Eq. (7b) is satisfied, the body continues to spin about its minor inertia axis x. Thus, in the case of a flat-spin recovery, the condition $E^* > E_{sep}$ states that the transition from a rotation about the maximum inertia axis (z) to a rotation about the minor inertia axis (x) has been accomplished.

In the presence of an arbitrary torque vector **T,** it follows from Eqs. (1a-c) that the rates of change of the rotational energy and angular momentum satisfy the equations:

$$\dot{E} = \boldsymbol{\omega} \bullet \mathbf{T}; \quad \dot{H} = \left(\mathbf{H} \bullet \mathbf{T}\right) / H \qquad (8a,b)$$

Thus, the energy remains unchanged if the torque vector acts perpendicular to the rotation vector. Similarly, the modulus of the angular momentum vector remains constant if the torque vector acts perpendicular to the angular momentum vector.

Torque about Minor Axis of Inertia

Here, we focus on the special case where only one of the torque components is non-zero, namely $t_1 > 0$, whereas $t_2 = t_3 = 0$. The torque acts along the *minor* inertia axis (x) and generates a positive spin-up. We distinguish between two types of initial conditions:

a) pure spin about the z-axis, which refers to a flat-spin situation with $\omega_{10} = \omega_{20} = 0$, $\omega_{30} = H_0/C$.
b) nutational motion about the z axis; this refers to a 'partial flat spin' with nutation angle ν and $E_{min} < E_0 < E_{sep}$.

When combining Eqs. (4b,c) and the definitions in Eqs. (5) for the present conditions we obtain the *first integral*:

$$\frac{d}{dt}\left(k_3\omega_2^2(t)+k_2\omega_3^2(t)\right)=0 \quad \Rightarrow \quad H^2(t)-2AE(t)=constant \tag{9a,b}$$

Although the rotational energy nor the angular momentum are conserved separately, *the linear combination in Eq. (9b) remains constant under a torque acting along the x-axis*. The existence of this first integral is crucial for simplifying the treatment of the problem at hand.

Alternatively, Eq. (9b) may be written as (see also Eq. 6):

$$\boxed{\Delta E(t)=\frac{H^2(t)}{2A}-E(t)=E_{max}(t)-E(t)} \tag{10a}$$

$$\Rightarrow \quad \Delta E=\frac{BC}{2A}\left(k_3\omega_{20}^2+k_2\omega_{30}^2\right)=constant>0 \tag{10b}$$

In the present case, ΔE stands for the (positive) difference between the maximum possible energy $E_{max} = H^2/(2A)$ that is compatible with the actual instantaneous angular momentum $H(t)$, and the actual instantaneous energy $E(t)$. Eqs. (10) provide a useful physical interpretation of the *first integral* of the system.

Similar first integrals exist when the torque acts along any of the other two axes but the physical interpretation will then be different. Also it may be noted that the first integral ΔE is similar to the first integral A^2 used in Ref. [8].

Obviously, Eq. (10b) is identical to the ellipse:

$$\frac{\omega_2^2(t)}{a^2}+\frac{\omega_3^2(t)}{b^2}=1 \tag{11}$$

with:

$$a=\sqrt{\frac{2A\,\Delta E}{B(B-A)}} \quad > \quad b=\sqrt{\frac{2A\,\Delta E}{C(C-A)}} \tag{12a,b}$$

In the special case when also $\omega_{20} = 0$ these expressions may be simplified as:

$$\Delta E=\frac{BC}{2A}k_2\omega_{30}^2 \quad \Rightarrow \quad a=\omega_{30}\sqrt{\frac{k_2}{k_3}} \quad > \quad b=\omega_{30} \tag{12c,d}$$

It follows that the axes a and b of the ellipse in Eq. (11) remain constant throughout the motion. The angular velocity vector $\boldsymbol{\omega}$ moves on a cylindrical surface with the ellipse of Eq. (11) as base. Therefore, the rotation components $\omega_2(t)$ and $\omega_3(t)$ may be parameterized as follows:

$$\boxed{\omega_2(t) = a\cos u(t); \quad \omega_3(t) = b\sin u(t)} \tag{13a,b}$$

The eccentric anomaly $u(t)$ of this ellipse is an unknown function of time at this stage.

Eqs. (11-13) are, of course, also valid in the case of torque-free motion with the following interpretation. Depending on the initial conditions, the angular velocity either revolves about the minor inertia axis (x), see Figure 2a, or about the major inertia axis (z), see Figure 2b. In the first case, the projection on the y,z-plane describes the ellipse of Eqs. (11) and u covers the full range from 0 to 2π. The angular velocity ω_1 about the x-axis keeps its sign while fluctuating between its minimum and maximum values or increases continuously if the recovery is achieved.

In the second case, it is the ω_3 component that fluctuates between its minimum and maximum values without changing sign. In the y,z-plane, ω_2 oscillates symmetrically about the z-axis and only a part of the ellipse is described while u stays within a symmetric range (u_{min}, u_{max}) about the z-axis. In torque-free motion, a transition between these two cases is not possible. The initial conditions (i.e., the values of E and H) determine which one of these two possibilities occurs. The separation between the two cases mentioned above is given by the condition $2EB = H^2$.

A similar situation applies when a torque $t_1 > 0$ acts about the x-axis. If the initial rotation is already about the x-axis, Eq. (8a) shows that $\dot{E} = \omega_1 t_1 > 0$ and the body spins up further. If the initial rotation is about the z-axis, only an arc of the ellipse is described. The presence of the torque t_1 may imply a transition to a spin-up about the x-axis. However, such a transition occurs only under certain specific conditions. Figure 3 provides a quantitative visualization of Figure 2b.

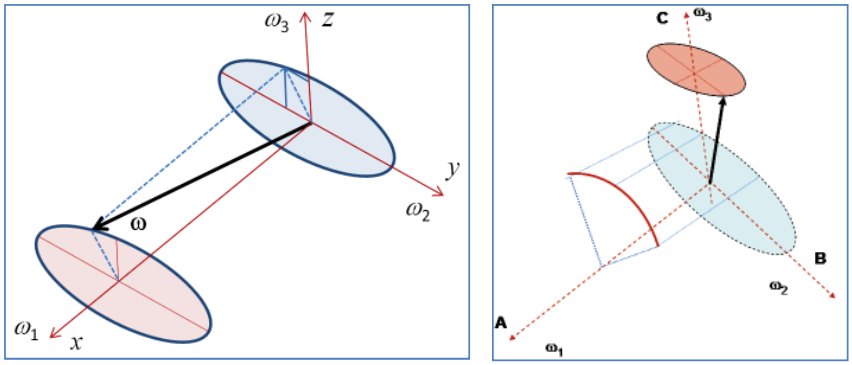

Figures 2. Motion of Angular Velocity Vector about a) Minor Axis x; b) Major Axis z.

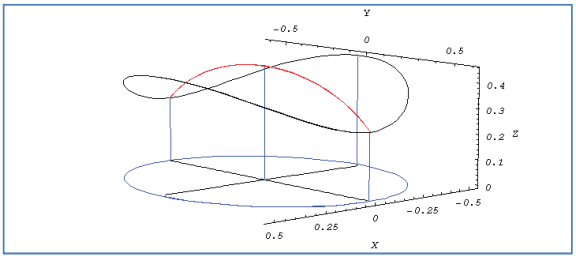

Figure 3. Quantitative Illustration of Large Nutation about z Axis.

By substituting Eqs. (13) in Eqs. (4b,c) with $t_2 = t_3 = 0$ we find the surprisingly compact result:

$$\boxed{\dot{u}(t) = -k\,\omega_1 \quad with: \quad k = \sqrt{k_2 k_3} = \sqrt{\frac{(B-A)(C-A)}{BC}}} \tag{14a,b}$$

where k denotes the ratio between the nutation frequency and the spin frequency for motion about the minor inertia axis (x). Whereas in Eqs. (13) the variable u serves as phase angle for the motion in the y,z-plane, in Eqs. (14) $u(t)$ is proportional to the total turning angle $\int \omega_1(\tau) d\tau$ about the x-axis.

The condition for an ongoing spin-up is that $\dot{u} < 0$ and never returns to zero. When $\dot{u} < 0$ the ellipse of Eqs. (13) is traced in the clockwise sense as is the case for a free nutation about the minor inertia axis. The projection of the angular velocity on the y,z-plane revolves on this ellipse.

Next, we focus on the rotational motion about the x-axis. After substituting Eqs. (13) into the first Euler Eq. (4a) we obtain the following 2nd order differential equation for the variable $u(t)$:

$$\boxed{\ddot{u}(t) - K_0 \sin\{2u(t)\} + k t_1 = 0} \tag{15a}$$

with:

$$K_0 = \left(\frac{C-B}{BC}\right)\Delta E = \frac{1}{2} k_1 \left(k_3 \omega_{20}^2 + k_2 \omega_{30}^2\right) \tag{15b}$$

Eq. (15a) has the structure of the forced nonlinear pendulum equation. After multiplying by $2\dot{u}$, we obtain a total differential and hence a *second* first integral:

$$(\dot{u})^2 + K_0 \cos(2u) + 2 k t_1 u = \Omega_c^2 = constant \tag{16a}$$

with initial conditions:

$$u_0 = \tan^{-1}\left(\sqrt{\frac{k_2}{k_3}}\frac{\omega_{30}}{\omega_{20}}\right); \quad \dot{u}_0 = -k\,\omega_{10} \tag{16b,c}$$

The constant Ω_c^2 in Eq. (16a) may be expressed in its known initial parameters as follows:

$$\Omega_c^2 = k^2 \omega_{10}^2 + \frac{k_1}{2}\left(k_3 \omega_{20}^2 - k_2 \omega_{30}^2\right) + 2 k t_1 u_0 \tag{17}$$

In contrast to the first integral ΔE, this second first integral depends on the initial rate ω_{10} and the torque level t_1. After substituting Eq. (14a), Eq. (16a) immediately produces the solution for $\omega_1^2(u)$ in terms of the integration constant Ω_c^2 in Eq. (17) and the parameter K_0 in Eq. (15b):

$$\boxed{\omega_1^2(u) = \frac{(\dot{u})^2}{k^2} = \frac{\Omega_c^2}{k^2} - \frac{K_0}{k^2}\cos(2u) - \frac{t_1}{k}(2u)} \tag{18}$$

The case $t_1 > 0$ can only lead to a *positive* spin-up about the x-axis so that $\omega_1(u)$ remains positive after a transition to a rotation about the minor axis of inertia. In the case of a partial flat spin, ω_1 may be negative initially. In this case, u initially increases but in its nutation about the z axis, $|\omega_1|$ will decrease and go through zero so that ω_1 becomes positive. When this happens u starts decreasing. Because Eq. (18) is unique, this implies that part of the curve of Eq. (18) is passed through twice. This will be illustrated in the results for a partial flat spin.

Finally, it is useful to express Eq. (18) in terms of the differences from the initial state:

$$\omega_1^2(u) - \omega_{10}^2 = \frac{K_0}{k^2}\left[\cos(2u_0) - \cos(2u)\right] + 2\frac{t_1}{k}(u_0 - u) \tag{19}$$

Perfect flat-spin motion is characterized by the fact that ω_{10} and ω_{20} vanish and the pure spin rate about the z axis is $\omega_{30} = H_0/C$ with H_0 the initial angular momentum. Eqs. (16b,c) show that $u_0 = \pi/2$ and $\dot{u}_0 = 0$ in this case. Subsequently, $u(t)$ decreases while $\omega_1(t)$ increases for $t > 0$. A sufficient condition for *flat-spin recovery* is that $\omega_1^2(u) = 0$ is the minimum value (if it occurs at all). When applying this condition to Eq. (19), we obtain the minimum torque level for recovery:

$$t_1 \geq \frac{K_0}{k}\sin(2u) = \frac{\Delta E}{I_{ref}}\sin(2u) \tag{20}$$

with the 'reference' inertia parameter I_{ref} defined by (see also Appendix A):

$$I_{ref} = k\left(\frac{BC}{C-B}\right) = \frac{\sqrt{(B-A)(C-A)BC}}{C-B} \tag{21}$$

The torque level in Eq. (20) is sufficient for guaranteeing spin-up about the minor inertia axis. In the case of an on-going spin-up, the fact that the sine term in Eq. (20) lies within the interval [-1, 1] leads to the following *sufficient* condition for a successful flat-spin recovery:

$$t_1 \geq \frac{\Delta E}{I_{ref}} \tag{22}$$

Thus, the condition on the torque level in Eq. (22) *depends only on the (initial) excess kinetic energy ΔE and the inertia parameter* I_{ref}.This result is consistent with the condition $A \geq \sqrt{2}$ specified in the text below Eq. (31) of Ref. [8].

It may be noted that the required torque level goes to zero for a symmetric body $B = C > A$ as $I_{ref} \to \infty$. Indeed, Eq. (1a) becomes decoupled from Eqs. (1b,c) and any $t_1 > 0$ guarantees a spin-up. For a nearly symmetric body ($B \approx C$), I_{ref} may still be large and a small torque may suffice for a recovery. Appendix A gives the values of $0 < I_{ref} < \infty$ for any possible rigid-body configuration.

RESULTS FOR FLAT-SPIN RECOVERY

Case 1: Starting from Perfect Flat Spin

For illustration, we consider a hypothetical satellite with the moments of inertia:

$$A = 200;\ B = 300;\ C = 400\ [\text{kg m}^2] \tag{23}$$

The initial flat-spin angular velocity about the maximum inertia axis (z) is taken as $\omega_{30} = 5$ [rpm], which corresponds to a 10 [rpm] spin about the minor inertia axis (x) prior to the flat-spin. The other two components vanish, i.e. $\omega_{10} = \omega_{20} = 0$, so that $u_0 = 90°$, see Eq. (16b). (These are typical parameters for a pure flat-spin situation.) These inputs lead to the following auxiliary parameters:

$$H_0 = 209.44\ [\text{Nms}];\ E_0 = 54.831;\ \Delta E = 54.831\ [\text{Nm}];\ \Omega_c^2 = 0.058324\ [\text{rad/s}^2] \tag{24}$$

For a perfect initial flat spin, the rate ω_1 starts increasing from zero (for a positive torque T_1) and needs to remain positive to guarantee recovery. Figure 4 illustrates the resulting evolutions of the angular velocity $\omega_1^2(u)$ for a few selected levels of T_1. The gyroscopic coupling due to the initial nutation about the z-axis may cause the curve $\omega_1(u)$ to return to zero.

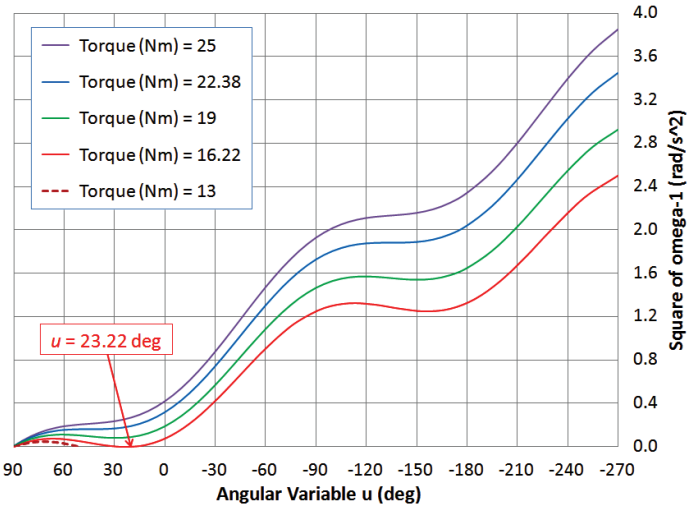

Figure 4. Recovery Options from Pure Flat Spin at 5 [rpm] about z-axis.

If the $\omega_1(u)$ curve actually *crosses* 0 at some point $u = u_{min}$ the range of u-values remains bounded within the interval $[u_{min}, u_0 = 90°]$. There will be no flat-spin recovery as the system continues its nutational motion about the z-axis. This case is illustrated by the dashed brown curve for $T_1 = 13$ [Nm] in Figure 4.

The red curve for $T_1 = 16.22$ [Nm] in Figure 4 shows the case when the curve $\omega_1(u)$ touches its zero line, which corresponds to the critical minimum torque T_1^* that enables a flat-spin recovery. Torques that satisfy $\omega_1(u) = 0$ follow from Eq. (19) by imposing $\omega_1^2(u) = 0$ and solving for t_1:

$$t_1(u) = \frac{k\omega_{10}^2}{2(u_0 - u)} + \frac{\Delta E}{I_{ref}}\left\{\frac{\cos(2u) - \cos(2u_0)}{2(u_0 - u)}\right\} \tag{25}$$

The maximum torque that satisfies Eq. (25) is the critical torque t_1^* with associated u^*. This torque t_1^* makes that the curve $\omega_1(u)$ touches zero at $u = u^*$ and then turn positive again. This implies that $\omega_1(u)$ in Eq. (19) must reach its minimum value at u^*, which leads to the condition that was already established in Eq. (20):

$$t_1^*(u^*) = \frac{\Delta E}{I_{ref}}\sin(2u^*) \tag{26}$$

An explicit equation for u^* can now be found by equating the conditions in Eqs. (25) and (26):

$$\cos(2u^*) - \cos(2u_0) + 2(u^* - u_0)\sin(2u^*) = 0 \tag{27}$$

which may be solved by iteration. In the present example, the result gives $u^* = 23.22°$. When substituting u^* into Eq. (26) we find the critical minimum torque $T_1^* = A\,t_1^* = 16.22$ [Nm].

Figure 5 illustrates the critical torque t_1^* as function of u^*. The left-hand part shows the first *maximum* of Figure 4 whereas the right-hand part corresponds to the first *minimum*. The critical torque 16.22 [Nm], which generates the red curve in Figure 4, is indicated. The maximum possible critical torque value is $T_1^* = 22.38$ [Nm], which corresponds to the blue $\omega_1(u)$ curve in Figure 4 that has a limiting horizontal tangent at $u^* = 45°$. For still larger torques the extrema disappear completely as shown by the purple $\omega_1(u)$ curve for $T_1 = 25$ [Nm] in Figure 4.

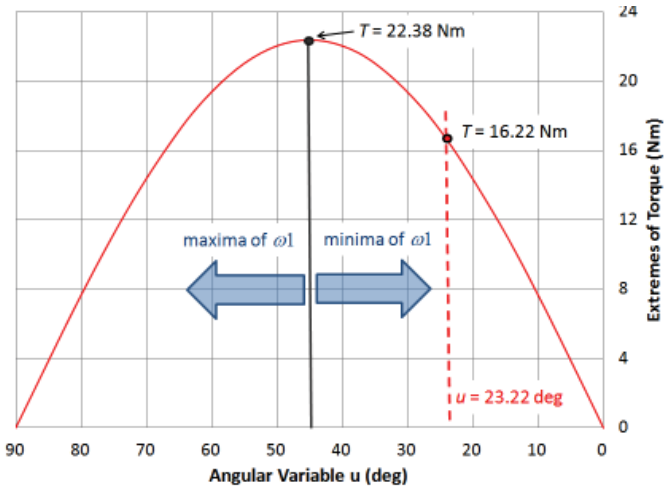

Figure 5. Critical Extreme Values of Torques T_1 as Function of u.

If the torque ceases to act when $\omega_1 = 0$ we have $\Delta E_{sep} = E_{sep} - E > 0$ and the corresponding free motion is still a nutation about the z-axis and the crossing of $\Delta E_{sep} = 0$ occurs later. The value u_{sep} can be calculated by substituting the results of Eqs. (13b) and (19) in $\Delta E_{sep} = 0$:

$$A(A-B)\omega_1^2(u_{sep}) + C(C-B)\omega_3^2(u_{sep}) = 0 \tag{28a}$$

$$\Rightarrow \quad u_{sep} = \frac{\pi}{2} - \sqrt{\frac{k_2}{k_3}}\frac{k_1\omega_{30}^2}{2t_1} \tag{28b}$$

For the data considered we find $u_{sep} = 10.93°$ at the transition to a spin about the minimum axis.

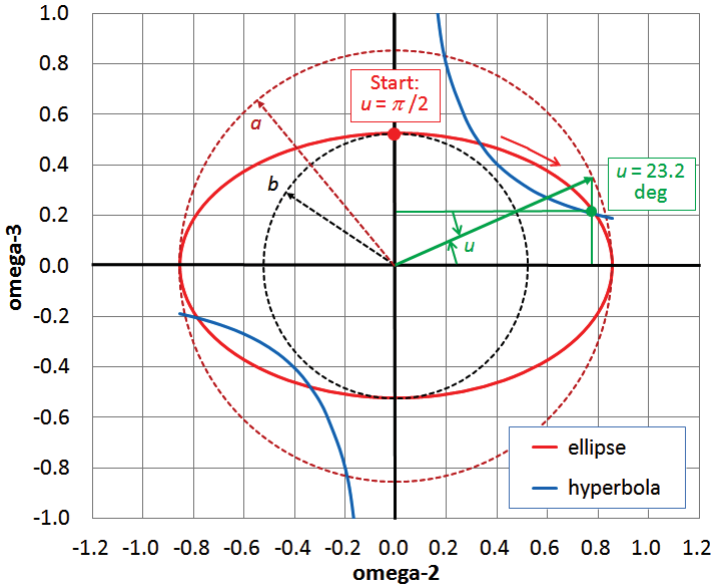

Figure 6. Projected ω Vector in the y,z-Plane as Function of u.

Figure 6 shows the motion in the y,z-plane. The variable u decreases from $\pi/2$ to the green line where $u = 23.2°$ and $\omega_1 = 0$. This point lies also on the hyperbola $\omega_2 \omega_3 = t_1/k_1$ which is the locus of the stationary solutions (i.e., $\dot{\omega}_1 = 0$, see Eq. 4a) together with $\omega_1 = 0$. When substituting Eqs. (13) into this hyperbola and comparing the result with Eq. (20) we find that the intersections correspond to u values where ω_1^2 reaches its extreme. This result illustrates the instability of the stationary solutions[1-3]. Since ω_1 increases again from this point onwards, the angle u in Figure 6 keeps decreasing. The transition to a spin about the x-axis is established at $u_{sep} = 10.93°$.

Case 2: Starting from Initial Nutation

In this case, there is initially a nutation about the maximum (z) axis. It is of interest to investigate whether the phasing of the nutation has an impact on the magnitude of the required recovery torque. The inertias and initial angular momentum are the same as in the flat-spin case but not the rotational energy. As initial conditions we consider the four cases A, …, D indicated in Figure 7. The initial rates will be selected such that all four cases have the same nutation.

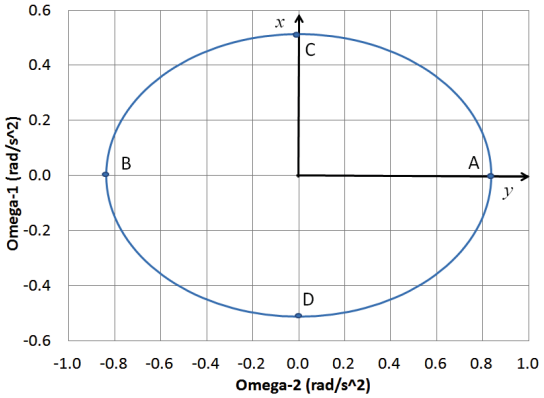

Figure 7. Initial Ellipse in x,y-Plane.

The points A and B have nutation phasing angles 0 and 180°, respectively, and $\omega_{10} = 0$. The initial nutation angle ν_0 is defined by:

$$\tan\nu_0 = \frac{B\omega_{20}}{C\omega_{30}} \quad \Rightarrow \quad \omega_{20} = \pm\frac{H_0}{B}\sin\nu_0\,; \quad \omega_{30} = \frac{H_0}{C}\cos\nu_0 \tag{29a-c}$$

$$E_0 = \frac{H_0^2}{2}\left\{\frac{\sin^2\nu_0}{B} + \frac{\cos^2\nu_0}{C}\right\} \quad with: \quad H_0^2 = B^2\omega_{20}^2 + C^2\omega_{30}^2 \tag{30a,b}$$

The points C and D in Figure 7 have phasing angles 90° and 270° and $\omega_{20} = 0$. The associated initial rates are found by imposing the same initial angular momentum and energy values H_0, E_0 of Eqs. (30). Two equations for the unknown initial rates ω_{10}, ω_{30} can be obtained from Eqs. (5):

$$A\omega_{10}^2 + C\omega_{30}^2 = 2E_0\,; \quad A^2\omega_{10}^2 + C^2\omega_{30}^2 = H_0^2 \tag{31a,b}$$

which leads to the following solutions:

$$\omega_{10} = \pm\sqrt{\frac{2CE_0 - H_0^2}{A(C-A)}}\,; \quad \omega_{30} = \sqrt{\frac{H_0^2 - 2AE_0}{C(C-A)}} \tag{32a,b}$$

Results of Simulations

Table 1 provides a summary of the results from the simulations of the four cases indicated in Figure 7. The first row summarizes the flat-spin results shown in Figure 4. The next 4 rows give the results for initial (maximum) nutation angles $\nu_{MAX} = 20°$. The general behavior of $\omega_1^2(u)$ is similar to that shown in Figure 4 with only 1 maximum and 1 minimum value for ω_1^2 in the case that the recovery takes place. Only the numerical values vary. The initial energy $E_0 = 56.969$ [Nm] is now higher than for the flat-spin case and one expects a priori that the recovery may be performed by a smaller torque. However, the initial nutation phase angle has a major impact on the recovery torque level.

Table 1 – Summary of Inputs and Results of Simulations.

$H_0 = 209.44$	**Case**	ω_{10}	ω_{20}	ω_{30}	u_0	$\Omega_c^2(t_1*)$	T_1*	$u(\omega_1=0)$
		[rad/s]			[deg]	[rad/s^2]	[Nm]	[deg]
Flat Spin		0	0	0.5236	90	0.05832	16.22	23.22
ν_{MAX} = 20°	1A	0	0.2388	0.4920	73.45	0.06253	18.98	30.95
	1B	0	-0.2388	0.4920	106.55	0.05032	11.47	16.12
$E_0 = 56.969$	1C	0.2070	0	0.5133	90	0.05385	14.12	20.53
$\Delta E = 52.693$	1D	-0.2070	0	0.5133	90	0.05385	14.12	20.53
ν_{MAX} = 60°	2A	0	0.6046	0.2618	35.26	0.05120	15.83	35.26
	2B	0	-0.6046	0.2618	144.74	0.03458	2.245	3.843
$E_0 = 68.539$	2C	0.5236	0	0.4534	90	0.03516	3.701	6.367
$\Delta E = 41.123$	2D	-0.5236	0	0.4534	90	0.03516	3.701	6.367

In case 1A the critical torque of 18.98 Nm is higher than the value required for a recovery from a perfect flat spin in spite of the fact that ω_1 starts also from zero and the energy required for recovery is smaller. The conclusions for case B are the opposite. The cases 1C and 1D have identical critical recovery torques, which is no surprise since Eq. (25) contains ω_{10} only in quadratic form. The torque is smaller than in the flat-spin case (i.e., 14.13 versus 16.22).

Figures 8 show the curve $\omega_1(u)$ with starting point $u_0 = 90°$ for both cases. Case 1C has $\omega_{10} > 0$ and u decreases from the start. In contrast, case 1D has $\omega_{10} < 0$ so u increases at first until $u_{max} = 96.11°$ where $\omega_1(u)$ crosses zero and starts decreasing. The value u_{max} follows also from $\omega_1^2(u) = 0$ but its derivative is not zero. *Only by combining the results of Eqs. (18) and (14a) can we establish which root of Eq. (18) corresponds to the actual motion.*

Similarly, the last 4 rows provide the results for initial (maximum) nutation angles $\nu_{MAX} = 60°$ and initial angular momentum H_0 as in the previous cases but with a still higher initial energy $E_0 = 68.539$ [Nm]. In the cases 2A and 2B, the initial rate $\omega_{10} = 0$ and ω_{20}, ω_{30} are calculated, as before, from Eqs. (29). For the cases 2C and 2D with $\omega_{20} = 0$ the approach of Eqs. (31-32) can be used again for calculating ω_{10}, ω_{30} (with the H_0 and E_0 values of cases 2A and 2B).

The results for the cases 2A, …, 2D in Table 1 confirm the trends for the critical recovery torque values as observed in the previous cases 1A, …, 1D. In particular, it follows that the recovery torque is highest when the initial angular velocity vector has the highest deviation *from the positive x-axis* (case A in Figure 7). The lowest torque occurs in cases B when the $\boldsymbol{\omega}$-vector deviation from the *negative x*-axis is highest. For the cases 2C and 2D the critical torques are again identical. They are much smaller than in the flat-spin case (i.e., 3.7 versus 15.8 Nm) and also compared to cases 1C, 1D. Again, the sign of ω_{10} has no influence on the results.

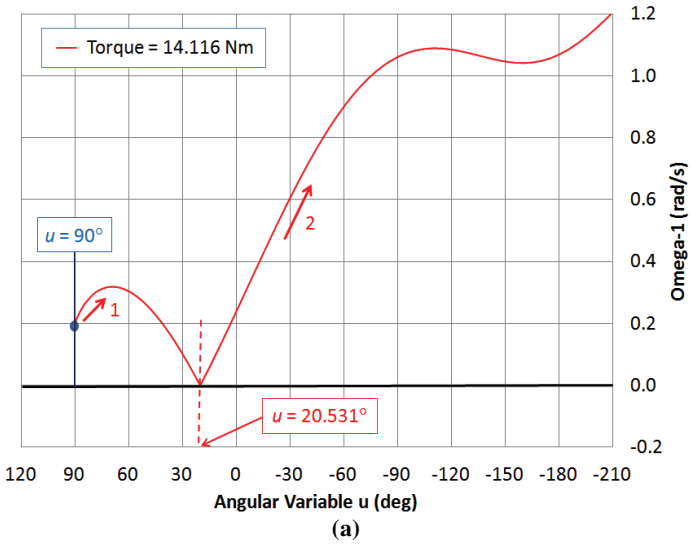

(a)

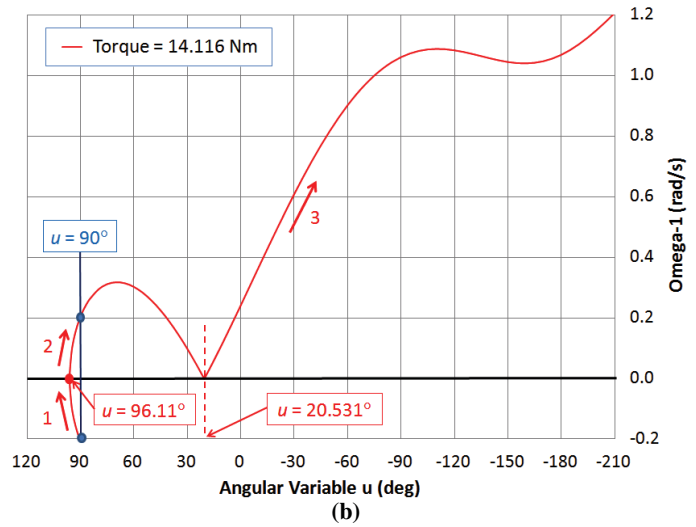

(b)

Figures 8. Evolution of $\omega_1(u)$ for ν_{MAX} = 20°: a) Case 1C; b) Case 1D.

Figure 9 provides a pictorial description of the satellite's spin-axis attitude evolution as it may occur in practice. Initially (picture on left), the satellite spins about its minor inertia axis (x), which is the nominal designated spin axis for performing its mission. Because of internal energy dissipation the satellite may end up in a flat-spin orientation where it rotates about its maximum inertia axis (z), which corresponds to its minimum-energy attitude[10] (two pictures on right).

Figure 9 shows that, during a flat-spin situation, the spin rate Ω_{spin} may be along either the $+z$ or $-z$ body axis depending on the location where the angular velocity did cross the separatrix during the energy dissipation phase (as indicated in the picture in the center of Figure 9).

Figures 10a,b illustrate the evolutions of the angular velocity components *within the body frame* for both $+z$ and $-z$ spin cases. The signs of ω_2 and ω_3 are inverted in Figures 10a,b but the spin rate about ω_1 is identical in both cases.

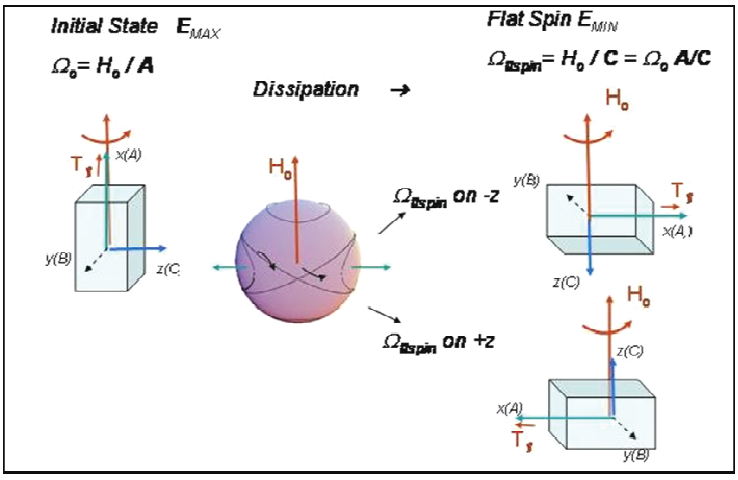

Figure 9. Visualization of Possible Flat-Spin Attitude Sequence.

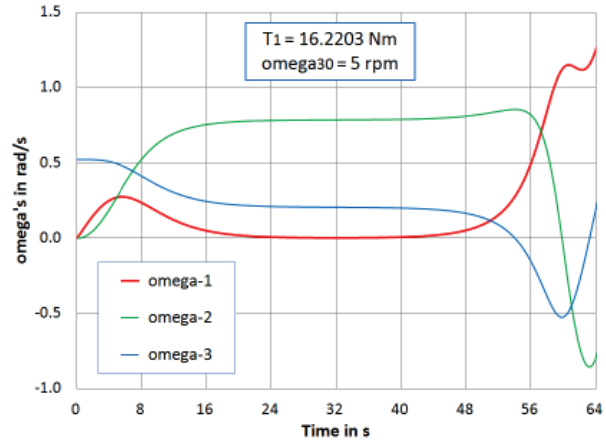

(a)

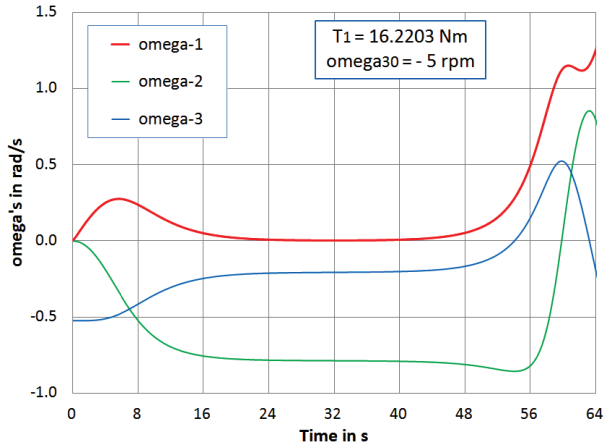

(b)

Figure 10. Flat-spin Recovery: a) for $\omega_{30} > 0$; b) for $\omega_{30} < 0$.

FORMULATION IN INDEPENDENT VARIABLE TIME

Numerical Analysis

The derivative $\dot{u}$ in Eq. (14a) gives the following result by means of separation of variables:

$$du / \sqrt{D(u)} = -dt \tag{33}$$

with $D(u)$ defined as follows, see Eq. (19):

$$D(u) = k^2 \omega_1^2(u) = k^2 \omega_{10}^2 + K_0 \left[\cos(2u_0) - \cos(2u)\right] + 2kt_1(u_0 - u) \tag{34}$$

If the last term of $D(u)$ in Eq. (34) were absent, Eq. (33) can be integrated in the form of an elliptic integral[13] for $u(t)$, which may have periodic solutions depending on the initial conditions. In general, the torque is non-zero and Eqs. (33-34) can only be solved by numerical methods.

By definition, the value of $D(u)$ must be positive. In the case when this condition imposes a restricted range of values for u, the solution oscillates with an average rotation that is still about the major inertia axis. Thus, the spin axis recovery does not take place in this case. On the other hand, when the condition $D(u) > 0$ imposes no lower limit on u, the projection of the angular velocity on the y,z plane revolves on the ellipse ΔE as discussed above.

Figure 11 shows the evolution of function $u(t)$ established by numerical integration of Eq. (33). The green line for $u = 23.22°$ indicates the level where $\omega_1(t)$ touches 0 and the blue line for $u = 10.93°$ indicates where the transition to a nutation about the x-axis occurs.

Figure 12 provides the comparison of the time evolutions for the three $\boldsymbol{\omega}$ components. As expected, the rates $\omega_2(t)$ and $\omega_3(t)$ vary periodically with different amplitudes. On the other hand, the rate $\omega_1(t)$ increases (since $t_1 > 0$) from zero and reaches a local maximum after about 5.6 [s] after which it returns to zero. After the transition, the slope of $\omega_1(t)$ becomes almost linear and approaches the value t_1 (which is the exact result for a symmetric body with $B = C$). This is a consequence of the fact that the rates ω_2, ω_3 remain on their fixed ellipse. Hence, their influence on ω_1 reduces gradually. This feature plays a role when interpreting the motion in inertial space.

Figure 13a shows the rates $\omega_j(t)$, $j = 1, 2, 3$, for the case when the torque T_1 is (marginally) too weak for a recovery, i.e. $T_1 = 16.22$. The angular rates as well as the function $u(t)$ in Figure 13b behave like periodic functions resembling the elliptic functions.

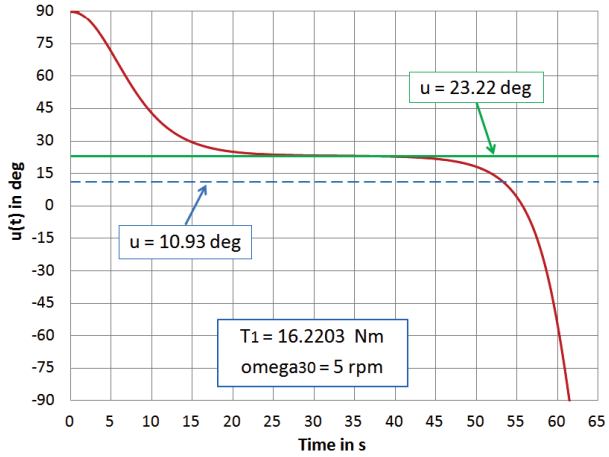

Figure 11. Function $u(t)$ for Recovery from Perfect Flat-Spin.

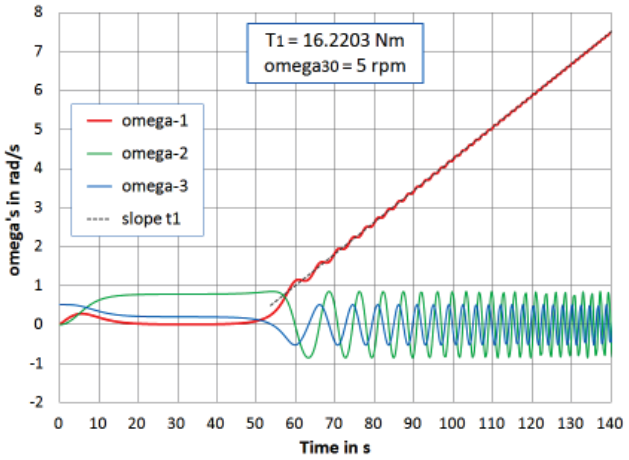

Figure 12. Functions $\omega_j(t)$, j = 1, 2, 3, for Flat-Spin Recovery.

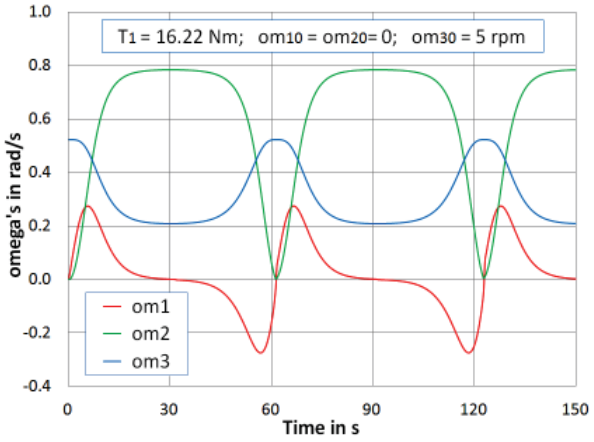

(a)

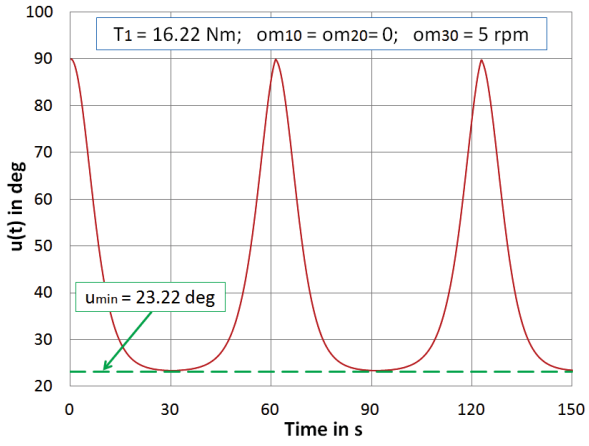

(b)

Figures 13. No Flat-Spin Recovery Case: a) Functions $\omega_j(t)$, j = 1, 2, 3; b) Function $u(t)$.

Approximate Analytical Model

The variable u crosses its zero value at the time $t_{u=0}$ = 55.66 [s] and decreases continuously afterwards (see Figure 11). For an initial pure flat spin (i.e., $\omega_{10} = \omega_{20} = 0$, $\omega_{30} = \Omega_0$) the value of $\omega_1(u{=}0)$ can be calculated from Eqs. (17-18):

$$\omega_{1(u=0)}^2 = \pi t_1 / k - k_1 \Omega_0^2 / k_3 \tag{35}$$

After inserting this expression into Eq. (34) and taking $u_0 = 0$ at time t_{u0} = 55.66 [s] as the initial conditions, we obtain the following result for $D(u)$:

$$D(u)_{(u=0)} = \pi k t_1 - k_1 k_2 \Omega_0^2 - 2k t_1 u + k_1 k_2 \Omega_0^2 \left\{\sin^2(u)\right\} \tag{36a}$$

$$\Rightarrow \quad \left\langle D(u)_{(u=0)} \right\rangle = \pi k t_1 - \frac{1}{2} k_1 k_2 \Omega_0^2 - 2k t_1 u \tag{36b}$$

where $\langle ... \rangle$ denotes the averaging operator.

Figure 14a shows the comparison of the two functions in Eqs. (36a,b). It shows that the averaged function is an adequate approximation of $D(u)_{(u=0)}$.

Next, we calculate an approximate solution for $u(t)$ by integrating (see Eq. 33):

$$\frac{du}{dt} \approx -\sqrt{\left\langle D(u)_{(u=0)} \right\rangle} \quad \Rightarrow \quad t - t_{u0} \approx -\int_0^u \frac{ds}{\sqrt{\left\langle D(s)_{(u=0)} \right\rangle}} \tag{37a,b}$$

Eq. (36b) shows that the denominator of the integrand takes the form $\sqrt{(e\text{-}fs)}$ with constants e and f. Thus, Eq. (37b) can be integrated analytically by elementary means. The result is an expression for $t - t_{u0}$ as a function of u. After inversion we obtain the following analytical result for $-u(t)$:

$$-u(t) = \sqrt{\left(\pi k t_1 - \frac{1}{2} k_1 k_2 \Omega_0^2\right)} (t - t_{u0}) + \frac{1}{2} k t_1 (t - t_{u0})^2 \tag{38}$$

Figure 14b shows the comparison of the 'approximate' result of the function u with the 'exact' numerical result shown in Figure 11 over the interval 60 to 140 seconds. The difference between the results increases gradually at an average rate of 0.02 [rad] per second over the interval.

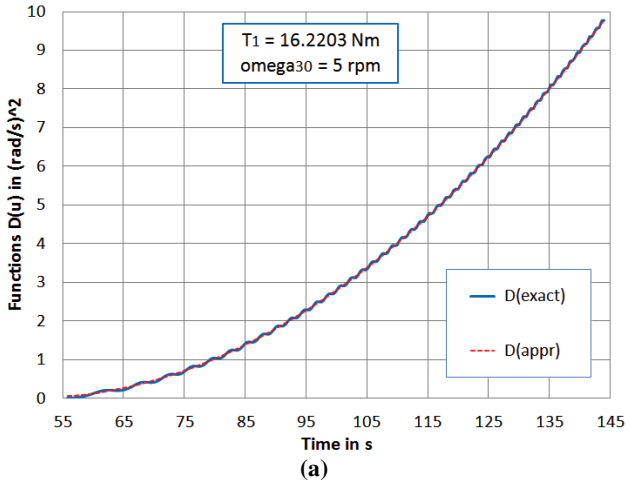

(a)

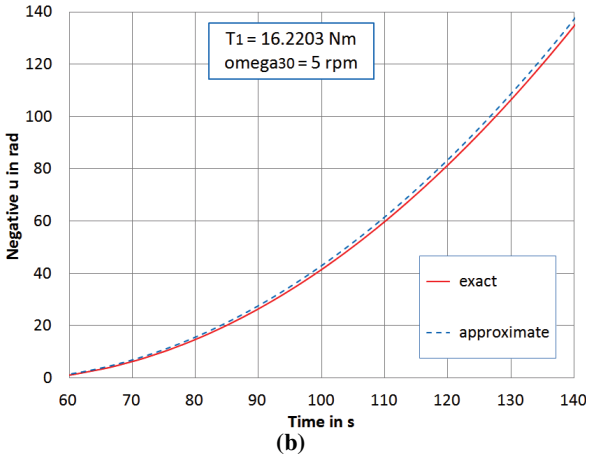

(b)

Figures 14. a) Function $D(u)$ and its Average; b) Numerical and Approximate Function $u(t)$.

EVOLUTION OF THE NUTATION

After its transition to a spin about the minor inertia axis (x), the satellite spins up while $-u$ increases continually (see Eq. 38 and Figure 4b). The nutation angle of this motion about the x-axis at the instant $u = 0$ is $\nu_{u0} = 70.68°$. This result follows by substituting Eqs. (12b) and (35) into the equation that defines the nutation angle:

$$\tan\left[\nu(u)\right] = \frac{h_{yz}}{A\,\omega_1(u)}; \quad with: h_{yz} = \sqrt{\left(h_y^2 + h_z^2\right)} \tag{39a,b}$$

This nutation decreases further with time as the projection of the angular momentum on the y,z-plane describes an ellipse with *constant* parameters a_{hy} and a_{hz}, which follows from Eqs. (13a,b):

$$a_{hy} = \sqrt{\frac{2AB\,\Delta E}{(B-A)}} \;>\; b_{hz} = \sqrt{\frac{2AC\,\Delta E}{(C-A)}} \tag{40a,b}$$

We present here a heuristic derivation of the average decrease of the nutation angle. Since the average values of $\cos^2(u)$ and $\sin^2(u)$ over the period $[0,-2\pi]$ are 0.5, the average value of h_{yz}^2 equals the constant:

$$\left\langle h_{yz}^2 \right\rangle = \frac{1}{2\pi}\int_{u_0}^{u_0-2\pi}\left\{h_{yz}^2(u)\right\}du = A\,\Delta E\left(\frac{B}{B-A}+\frac{C}{C-A}\right) \tag{41}$$

First, we approximate:

$$\left\langle \left|h_{yz}\right| \right\rangle \approx \sqrt{\left\langle h_{yz}^2 \right\rangle} \tag{42}$$

This equation is not exact because, in general, the average value of a quantity is not equal to the square root of the average of the square of that quantity. This procedure replaces the elliptic motion in the y,z-plane by a circular motion. After introducing $\left\langle \left|h_{yz}\right| \right\rangle$ in the definition of the nutation angle $\nu(u)$ (as in Eq. 39a), we find the following approximate result for the evolution of the nutation angle:

$$\left\langle \tan\left[\nu(u)\right] \right\rangle \approx \frac{\left\langle \left|h_{yz}\right| \right\rangle}{A\,\omega_1(u)} \tag{43}$$

Furthermore, because $|u|$ increases with time, we may neglect the periodic $(K_0/k^2)\cos(2u)$ term in Eq. (18) in comparison to the term $2t_1|u|/k$. This eliminates the fast oscillations in $\omega_1(u)$ and we are left with $< \omega_1 >$. A useful approximation for the nutation angle $\nu(u)$ follows then from:

$$\langle \nu(u) \rangle \approx \arctan\left(\frac{\langle |h_{yz}| \rangle}{A \langle \omega_1(u) \rangle} \right) \tag{44}$$

Figure 15 shows that Eq. (44) is effective in smoothing the fast oscillations of $\nu(u)$ while the frequency of the motion in the y,z-plane keeps increasing.

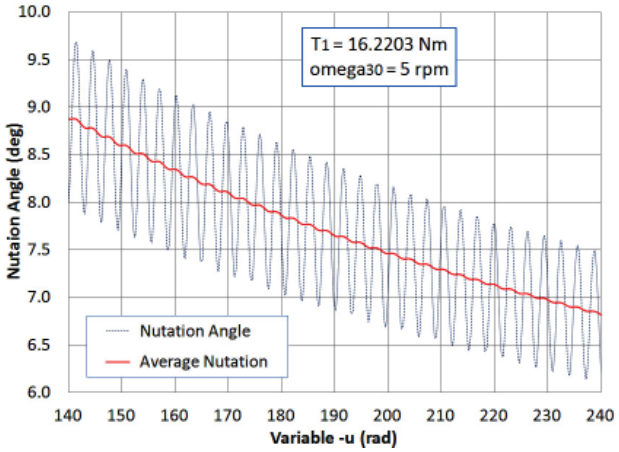

Figure 15. Close-up of Actual and Average Nutation Angle.

CONCLUSIONS

This paper investigates the flat-spin recovery performed by a continuous torque about the minor axis of inertia, which is the designated spin axis. The use of a first integral on the Euler equations for this problem allows a straightforward treatment of the dynamics within the principal body frame. The solution is formulated in terms of the total turning angle about the spin-up axis. This angle also describes the motion on a constant ellipse in the plane perpendicular to the spin axis. Explicit results for the torque required for a recovery and the decrease of the nutation are obtained. The evolution in time is described by a generalized pendulum equation which has no known analytical solution.

REFERENCES

[1] U. T. Bödewadt, "Der Symmetrische Kreisel bei Zeitfester Drehkraft." *Mathematische Zeitschrift*, Vol. 55, pp. 310-320, 1952.

[2] R. Grammel, "Die Stationären Bewegungen des Selbsterregten Kreisels und ihre Stabilität." *Ingenieur-Archiv*, Vol. XXI, No. 3, pp. 149-156, 1953.

[3] R. Grammel, "Der Selbsterregten Unsymmetrische Kreisel." *Ingenieur-Archiv*, Vol. XXII, No. 2, pp. 73-97, 1954.

[4] E. Leimanis, "The General Problem of the Motion of Coupled Rigid Bodies About a Fixed Point." Springer, New York, 1965.

[5] J. C. van der Ha, "Perturbation Solution of Attitude Motion under Body-Fixed Torques." *Acta Astronautica*, Vol. 12, No. 10, October 1985, pp. 861-869.

[6] J.M. Longuski and P. Tsiotras, "Analytical Solutions for a Spinning Rigid Body Subjected to Time-Varying Body-Fixed Torques - Part I Constant Axial Torques." *Transactions of ASME*, Vol. 60, December 1993, pp. 970-975.

[7] J.M. Longuski and P. Tsiotras, "Analytical Solution of the Large Angle Problem in Rigid-Body Attitude Dynamics." *The Journal of the Astronautical Sciences*, Vol. 43, No. 1, January1995, pp. 25-46.

[8] R. Livneh and B. Wie, "New Results for an Asymmetric Rigid Body with Constant Body-Fixed Torques." *Journal of Guidance, Control, and Dynamics*, Vol. 20, No. 5, September-October 1997, pp. 873-881.

[9] R. Livneh and B. Wie, "Asymmetric Body Spinning Motion with Energy Dissipation and Constant Body-Fixed Torques." *Journal of Guidance, Control, and Dynamics*, Vol. 22, No. 2, March-April 1999, pp. 322-328.

[10] C. D. Rahn and P.M. Barba, "Reorientation Maneuver for Spinning Spacecraft." *Journal of Guidance, Control, and Dynamics*, Vol. 14, No. 4, July - August 1991, pp. 724-728.

[11] M. Kaplan, "Modern Spacecraft Dynamics & Control." *Wiley*, New York, 1976, Section 2.3.6.

[12] D. L.Cronin, "Flat Spin Recovery of a Rigid Asymmetric Spacecraft." *Journal of Guidance and Control,* Vol. 1, No. 4, July - August 1978, pp. 281-282.

[13] P.C. Hughes, "Spacecraft Attitude Dynamics." *Dover Publications*. Mineola, NY, 2004, pp. 105-108.

[14] Wertz, J. (Editor), "Spacecraft Attitude Determination and Control." *Springer Scientific + Business Media, Berlin and New York*, 1978, pp. 765.

APPENDIX A – INTERPRETATION OF I_{REF}

The *reference moment of inertia* I_{ref} depends only on the shape of the body as can be seen from its definition in Eq. (21). In a diagram with axes$\{x = A/C,\ y = B/C\}$, the loci of constant values for I_{ref} are given by the curves:

$$x^2 y - x y^2 + (1 - I_{nor}^2)\, y^2 - x y + 2\, I_{nor}^2\, y - I_{nor}^2 = 0 \tag{A.1}$$

with the *normalized reference inertia* I_{nor} defined by:

$$I_{nor} = \frac{I_{ref}}{C} \tag{A.2}$$

The results are summarized in Figure A.1. Feasible inertia configurations are contained within the triangular region bordered by the black border lines.

For an oblate body $A = B$ or $x = y$, Eqs. (21-22) show that $I_{ref} = 0$ and $t_1 \to \infty$ so that a flat-spin recovery is not possible. Furthermore, the ω_3 component is constant in this case. When $B > A$, the reference inertia I_{ref} increases and passes through A and B, corresponding to the curves $I_{nor} = A/C$ and B/C, respectively. For a prolate body $B = C$ or $y = 1$, $I_{ref} \to \infty$ and $t_1 \to 0$. Indeed, Eqs. (1) show that ω_1 remains decoupled from the other two components and increases linearly with time.

Figure A.1 also shows the region where I_{ref} lies within the range $\{A,C\}$, namely in-between the curves $I_{nor} = A/C = 0.5$ and $I_{nor} = 1$.

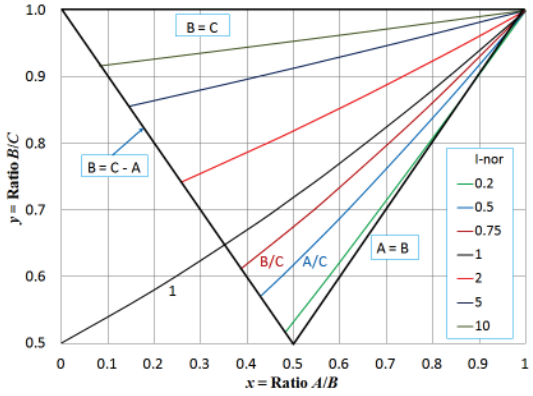

Figure A.1. Curves with Constant I_{ref} Values.